PHOTONICS Research

Numerical simulation and temporal characterization of dual-pumped microring-resonator-based optical frequency combs

Xiaohong Hu,[1,2,†] Weiqiang Wang,[1,2,3,†] Leiran Wang,[1,2] Wenfu Zhang,[1,2,3,4] Yishan Wang,[1,5] and Wei Zhao[1]

[1]State Key Laboratory of Transient Optics and Photonics, Xi'an Institute of Optics and Precision Mechanics, Chinese Academy of Science, Xi'an 710119, China
[2]University of Chinese Academy of Sciences, Beijing 100049, China
[3]China-UK Joint Research Center on Micro/Nano Photonics, Xi'an Institute of Optics and Precision Mechanics, Chinese Academy of Science, Xi'an 710119, China
[4]e-mail: wfuzhang@opt.ac.cn
[5]e-mail: Yshwang@opt.ac.cn

Received 10 February 2017; revised 21 March 2017; accepted 22 March 2017; posted 22 March 2017 (Doc. ID 286540); published 18 April 2017

Dual-pumped microring-resonator-based optical frequency combs (OFCs) and their temporal characteristics are numerically investigated and experimentally explored. The calculation results obtained by solving the driven and damped nonlinear Schrödinger equation indicate that an ultralow coupled pump power is required to excite the primary comb modes through a non-degenerate four-wave-mixing (FWM) process and, when the pump power is boosted, both the comb mode intensities and spectral bandwidths increase. At low pump powers, the field intensity profile exhibits a cosine variation manner with frequency equal to the separation of the two pumps, while a roll Turing pattern is formed resulting from the increased comb mode intensities and spectral bandwidths at high pump powers. Meanwhile, we found that the power difference between the two pump fields can be transferred to the newly generated comb modes, which are located on both sides of the pump modes, through a cascaded FWM process. Experimentally, the dual-pumped OFCs were realized by coupling two self-oscillating pump fields into a microring resonator. The numerically calculated comb spectrum is verified by generating an OFC with 2.0 THz mode spacing over 160 nm bandwidth. In addition, the formation of a roll Turing pattern at high pump powers is inferred from the measured autocorrelation trace of a 10 free spectral range (FSR) OFC. The experimental observations accord well with the numerical predictions. Due to their large and tunable mode spacing, robustness, and flexibility, the proposed dual-pumped OFCs could find potential applications in a wide range of fields, including arbitrary optical waveform generation, high-capacity optical communications, and signal-processing systems.

OCIS codes: (190.4380) Nonlinear optics, four-wave mixing; (190.4390) Nonlinear optics, integrated optics; (190.4970) Parametric oscillators and amplifiers; (140.3945) Microcavities.

https://doi.org/10.1364/PRJ.5.000207

1. INTRODUCTION

Microresonator-based Kerr optical frequency combs (OFCs) are an intriguing choice in applications such as arbitrary optical waveform generation [1] and astronomical spectroscopy [2] due their essential advantages of compactness, low cost, and especially their large obtainable mode spacing. Since the first demonstration of Kerr OFC generation from a silica toroidal microcavity [3], OFCs have been successfully achieved in various platforms, including doped silica glass [4], aluminum nitride [5], and silicon nitride [6].

Generally, Kerr OFC is realized by pumping a high-Q microresonator with a single continuous-wave (CW) field that is resonantly coupled into the microcavity. A special degenerate case of four-wave mixing (FWM) called modulation instability was found to be the main mechanism for the creation of the primary comb modes or sidebands, and is the most important frequency-conversion process in a microresonator [7]. The interactions of dispersion and Kerr nonlinearity determine the field profile, frequency span, and stability of the generated OFC. Nonlinear Schrödinger equation [8,9], modal

expansion approach [10], and coupled-mode equation models [11] were used to simulate the formation process and obtain a better understanding of the OFC formation mechanism. Meanwhile, the Lugiato–Lefever equation was widely used as an effective tool to explore the spatiotemporal evolution of OFCs in microresonators [12,13]. It is worth noting that, to excite an OFC in a microresonator, a threshold for the intracavity pump field exists when the single-pumped scheme is adopted. Specifically, only when the power of the intracavity pump field exceeds the threshold value can an OFC be generated [13]. Meanwhile, it is found that this threshold is inversely proportional to Q^2 [14]. An alternative pump configuration involves simultaneously coupling two CW fields into the microresonator. Theoretical analyses have revealed that the dual-pumped configuration allows for OFC generation through the nondegenerate FWM of the two pump modes even when the single-pumped configuration would correspond to a stable CW solution [15]. An additional merit of this pump scheme is that it provides an additional tuning degree of freedom in the form of the modulation frequency, which is much harder in the single-pumped approach. Up to 10 free spectral range (FSR, 135.6 GHz) OFC was experimentally obtained in a whispering gallery mode fluorite resonator using the dual-pump scheme [16]. However, as a result of the low pump power, only an OFC with a narrow bandwidth (~16 nm) was observed. Unlike the cavity-less cases [17,18], it is actually much more difficult to couple two pump waves into the microcavity simultaneously because of the thermal effects that induce resonance shifting. Evidently, this resonance shifting is also the main limitation to the generation of broadband OFCs by further increasing the pump power. Dual-pumped OFCs with increased bandwidths were demonstrated recently by injecting two self-oscillated pump fields into a microring resonator (MRR), and comb spectra with varying mode spacing were realized [19]. In addition to OFC generation, a dual-pumped degenerate parametric oscillator was also realized [20]. Specifically, frequency degenerate signal and idler fields were produced by coupling two frequency-detuned pump waves into a silicon nitride microresonator with normal dispersion.

In this paper, we numerically investigate the characteristics of dual-pumped OFCs generated from a CMOS-compatible high-Q MRR. Theoretical analyses are performed by solving the nonlinear driven and damped Schrödinger equation via standard split-step Fourier method. The comb spectra and field intensity profiles at different pump powers are present. Meanwhile, the effect of intensity difference between the pump fields is also studied. The numerical predictions, including the spectral and temporal characteristics of dual-pumped OFCs, are further verified through the experimentally measured comb spectra and autocorrelation trace.

2. NUMERICAL SIMULATION AND DISCUSSION

Figure 1(a) shows the dual-pumped OFC generation process. As shown in the figure, when two pump fields are injected into an MRR simultaneously, an optical spectrum with a comb structure can be generated through the FWM process in the MRR. The energy diagram of the non-degenerate FWM process is

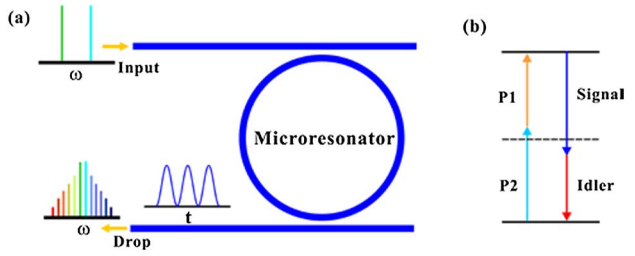

Fig. 1. (a) Schematic diagram of dual-pumped OFC generation system. The two pump fields are coupled into a four-port MRR through the input port, and the generated OFC is measured at the drop port. (b) Energy diagram of non-degenerate FWM in the MRR.

shown in Fig. 1(b). Compared with the degenerate FWM process in the single-pumped case, the non-degenerate FWM is expected to be much more efficient as a result of the simultaneously injected pump fields and increased pump power. The microresonator reported here is a passively integrated, four-port, high-index doped silica glass MRR with FSR of 49 GHz and Q factor of $\sim 1.45 \times 10^6$ at 1550 nm [19].

Theoretically, field evolution and OFC generation from a dual-pumped microresonator can be described using the mean-field driven and damped nonlinear Schrödinger equation given by [17]

$$\tau_0 \frac{\partial A}{\partial \tau} = -(\alpha + i\delta_0)A + i\gamma L|A|^2 A - i\frac{\beta_2 L}{2}\frac{\partial^2 A}{\partial t^2} + \sqrt{T_c}A_{in}, \tag{1a}$$

$$A_{in}(t) = \sqrt{P}\left\{\sqrt{r}\exp[i(w_{p1} - w_0)t] + \sqrt{1-r}\exp[i(w_{p2} - w_0)t]\right\}. \tag{1b}$$

Here, $A(\tau, t)$ is the slowly varying envelope of the total intracavity field. The slow time parameter τ describes the evolution of the intracavity field over successive round-trips and the fast time scale t describes the temporal profile of the field. $\alpha = (\alpha_i L + T_c)/2$ is the loss per cavity round-trip including the intrinsic and coupling loss. The parameter δ_0 represents the average phase detuning of the two pumps. The second item on the right-hand side of Eq. (1a) describes the intensity-dependent nonlinear Kerr effect with γ being the nonlinear parameter. The second-order or group-velocity dispersion (GVD) is represented by the parameter β_2. Parameters τ_0, L, and T_c are the cavity round-trip time, cavity length, and power coupling coefficient, respectively. The pump fields are expressed by Eq. (1b) and, in order to reflect the power difference between the two pumps, we introduce an additional parameter r. The total pump power in the straight coupling waveguide is denoted by P. The angular frequencies, together with the average frequency of the two pump fields, are expressed by the parameters w_{p1}, w_{p2}, and w_0.

The field evolution and multi-FSR Kerr OFC generation is studied by numerically solving Eq. (1a) based on the physical parameters of the MRR listed in Table 1. The dispersion property of the MRR is investigated by considering both the material dispersion and ring-cavity-induced waveguide

Table 1. Physical Parameters of the MRR

Item	Symbol	Value
Quality factor	Q	1.45×10^6
Cavity length	L	3.72 mm
Mode field area	A_{eff}	~4.8 μm^2
Mode linewidth	κ	~134 MHz
Refractive index	n_0	1.6
FSR	FSR	49 GHz
Finesse	F	~367
Nonlinearity	γ	110 W^{-1} km^{-1}
GVD	β_2	−25 ps^2/km
Linear propagation loss	α_{dB}	~0.06 dB/cm
Power coupling coefficient	T_c	1.2×10^{-2}

Note: the parameters are accurate for 1.55 μm wavelength.

dispersion. The calculated GVD curve is shown in Fig. 2 and the MRR shows anomalous dispersion at pump wavelengths of around 1560 nm. Figure 3 presents the calculated field intensity profiles and their corresponding comb spectra. In order to compare them with the experimental results, the wavelengths of the two pump fields are set as 1551.26 and 1567.54 nm, corresponding to a frequency separation of 40 FSR. The GVD parameters of −25.25 and −27.63 ps^2/km are inferred from Fig. 2. The single-pumped case ($r = 0$) is also shown for comparison. As shown in Fig. 3, when the pump power in the coupling waveguide is 8 dBm, no comb spectrum can be formed and the initial field evolves to a stable homogeneous state in the single-pumped situation. This is because, for the selected pump strength, the intracavity field intensity is well below the threshold of modulation instability and the MRR supports only a homogeneous CW state. On the contrary, when a second pump field with a central wavelength of 1567.54 nm is introduced, a spectral profile with a comb structure is generated through the non-degenerate FWM process in the MRR. When the pump power is further boosted, both the spectral bandwidth and intensities of the comb modes increase. Meanwhile, at low pump powers, the field intensity profile exhibits a cosine variation manner, with the frequency equal to the separation of the two pumps. This is because the intensities of the newly generated comb modes, which are located on both sides of the two pumps, are much smaller than those of the

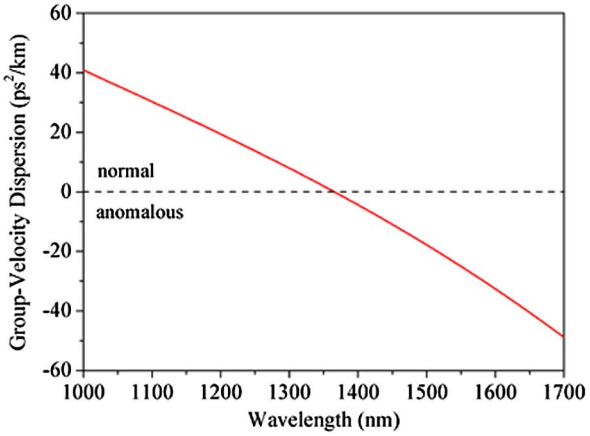

Fig. 2. Calculated GVD curve of the MRR used in the experiment.

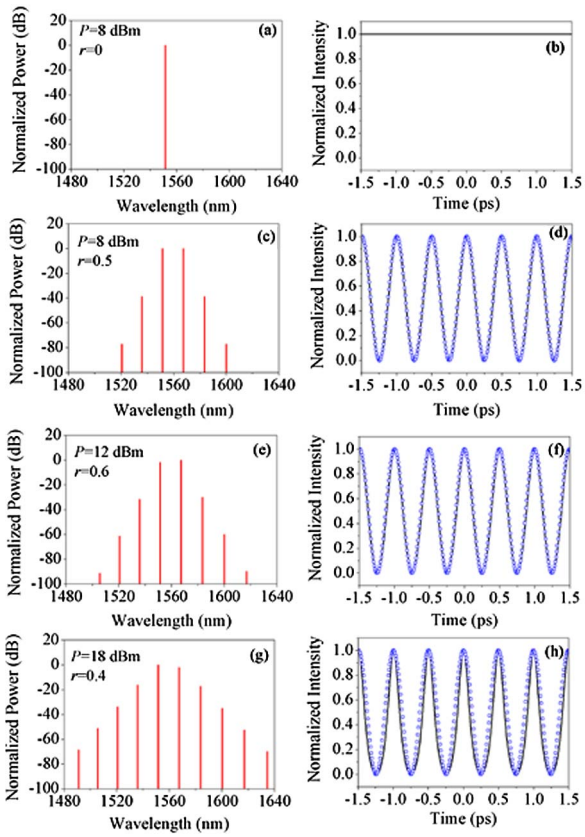

Fig. 3. Numerically calculated 40 FSR comb spectra (left column) and field profiles (right column) at different pump powers. For clear viewing, only a part of the field profile is shown at each pump power. A cosine fit to the field intensity profile is exhibited as the blue circles.

pump modes. Therefore, the temporal pattern is mainly determined by the beating of the two pump fields. As a result of increased spectral bandwidth and comb mode intensities, the field profile deviates gradually from the cosine variation manner and exhibits as a roll Turing pattern [13] with the further increase of pump power. Moreover, the effect of power difference between the two pump fields is also studied by changing the value of parameter r during the calculation process. It is found that the intensity difference of the pump modes can be transferred to the newly generated comb modes through a cascaded FWM process. In addition, it is worth mentioning that the adopted pump powers during the calculation process are below the optical parametric oscillation (OPO) threshold, which is around 22 dBm [19].

3. EXPERIMENTAL RESULTS

Figure 4 exhibits the experimental setup of the dual-pumped OFC system. As shown in the figure, the four-port MRR is simply embedded in a fiber loop cavity containing an erbium-doped fiber amplifier (EDFA) acting as the gain medium, a polarization controller (PC) controlling the field polarization in the laser loop, a programmable filter, and a delay line. The programmable filter with 0.4 nm bandwidth is a commercial WaveShaper produced by Finisar. In our experiment,

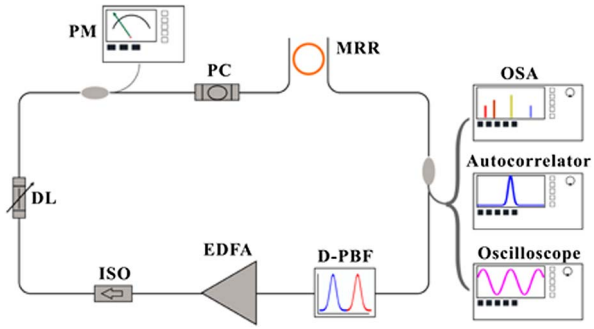

Fig. 4. Schematic diagram of the self-locked and dual-pumped OFC generation system. ISO, isolator; DL, delay line; D-PBF, dual passbands filter; OSA, optical spectrum analyzer; PM, power meter.

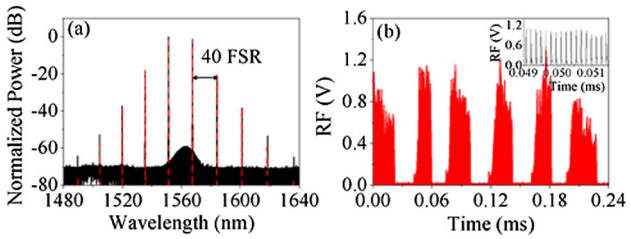

Fig. 6. (a) 40 FSR comb spectra. The experimentally measured and numerically calculated comb spectra based on Eq. (1a) are represented by the black solid and red dashed lines, respectively. (b) MRR output temporal intensity waveform measured with a fast photodetector. The inset shows the details of the temporal waveform resulting from the supermode beating.

it was used as a dual-band bandpass filter with the center wavelength tunable. The delay line, together with the PC, was employed to control the phase of the main cavity modes relative to the MRR modes, similar to filter-driven FWM mode-locked lasers [21]. The MRR was fabricated using a CMOS-compatible process [22,23] and pigtailed using a standard fiber array with less than 1 dB/facet coupling loss. In the OFC-generation experiment, the device acted as both nonlinear medium for cascaded FWM generation and finesse filter to select the pump wavelengths together with the programmable filter. The total power of the dual pump fields at the input port of MRR was monitored by a power meter, and the generated OFC was measured by a series of devices at the drop port of the MRR through a splitter. The total length of the main laser cavity is about 27 m, yielding an FSR of ~7.8 MHz.

In our experiment, the dual-pumped configuration was realized using the programmable filter. For simplicity, the central wavelength of one passband is fixed at 1567.53 nm. The power of the two pump fields was adjusted by tuning the gain of the EDFA. Once the pump fields oscillated stably in the MRR, two new frequencies were symmetrically excited on both sides of the pump modes through the non-degenerate FWM process. More and more comb modes were generated successively through cascaded FWM processes with the further increase of pump power. As an example, Fig. 5 shows the measured 10 FSR mode-spacing comb spectrum with an over 200 nm wavelength span when the pump power in the straight coupling waveguide reaches ~22 dBm. The pump wavelengths and mode spacing are 1563.5 nm, 1567.54 nm, and 0.5 THz, respectively. In addition, it can be inferred from the autocorrelation trace

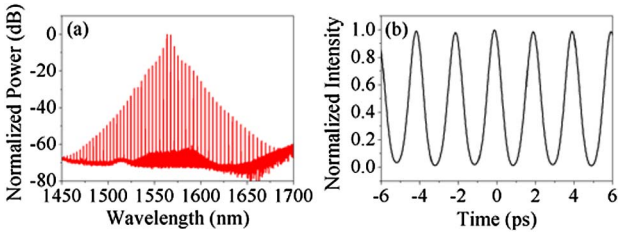

Fig. 5. Experimentally measured (a) 10 FSR comb spectra and (b) the corresponding autocorrelation trace.

shown in Fig. 5(b) that the field intensity profile exhibits as a roll Turing pattern.

In order to facilitate comparison with the numerically calculated comb spectrum, an OFC with large mode spacing was also realized in the experiment by varying the frequency separation of the two pump fields. Explicitly, Fig. 6(a) shows the measured and calculated 40 FSR (2 THz) mode-spacing comb spectra with an over 160 nm bandwidth. In this case, the pump power in the straight coupling waveguide is around 18 dBm and the pump wavelengths are 1551.26 and 1567.54 nm, respectively. A value of 0.4231 for the parameter r was inferred from the experimentally measured comb spectrum and adopted in the calculation to describe the effect of the intensity difference between the two pump fields. As shown in the figure, the calculated comb spectrum accords well with the experimental observation. Moreover, it should be mentioned that the main laser works in a classic Q-switching regime driven by supermode beating [24]; the measured MRR output intensity waveform is presented in Fig. 6(b). In this regime, on the one hand, supermode instability occurs because more than one main cavity mode can oscillate simultaneously within each MRR resonance, and the research results of the OPO process in an MRR showed that this instability may have an effect on enhancing the peak intensity of the intracavity optical field that, in turn, results in a stronger nonlinear process in the MRR [4]. On the other hand, to eliminate this supermode instability, improving the Q factor of the MRR or shortening the main cavity length until only one main cavity mode is allowed to oscillate within each MRR resonance are each expected to be effective methods for making the OFCs work in a more stable regime [19].

4. CONCLUSION

Temporal and spectral characteristics of dual-pumped MRR OFCs are investigated numerically and verified experimentally. Compared with single-pumped schemes, primary comb modes can be excited at a low pump power through nondegenerate FWM in the MRR. As a result of the high-intensity contrast between the pump fields and newly generated comb modes, the temporal field intensity profile exhibits a cosine variation manner at low pump powers. Instead, when the pump power increases, a roll Turing pattern forms as a result of the enhanced

comb mode intensities and frequency bandwidths. Meanwhile, it was found that the intensity difference between the symmetrically generated comb modes originates from the power difference of the two pump fields. When the pump power levels are below the OPO threshold, the calculated comb spectra based on Eq. (1a) accord well with the experimentally measured ones. In addition, the measured autocorrelation trace indicates that the field intensity profile deviates from a cosine variation manner, and a roll Turing pattern forms at high pump powers. Compared with a previously reported bichromatic pumping scheme [16], much higher pump power and thus a broad comb spectral bandwidth was achieved by using the self-oscillated scheme. Meanwhile, an alternative method to vary the mode spacing of microresonator-based Kerr frequency combs is through intentionally introduced mode interaction with a controllable location. Based on the coupled-microring structure, the frequency location of the mode interaction and comb mode spacing was changed by adjusting the integrated heater power of the auxiliary microring [25]. Compared with the self-locked dual-pump method presented here, a higher pump power and precise control of the heat power was required. The stability of the reported OFCs can be further improved by shortening the main laser cavity length to suppress the supermode instability.

Funding. Strategic Priority Research Program of the Chinese Academy of Sciences (CAS) (XDB 24030600); National Key Research and Development Program of China (2016YFF0200702); National Natural Science Foundation of China (NSFC) (61690222, 61308037, 61635013); CAS-SAFEA International Partnership Program for Creative Research Teams.

[†]The authors contributed equally to this work.

REFERENCES

1. S. T. Cundiff and A. M. Weiner, "Optical arbitrary waveform generation," Nat. Photonics **4**, 760–766 (2010).
2. T. Steinmetz, T. Wilken, C. Araujo-Hauck, R. Holzwarth, T. W. Hänsch, L. Pasquini, A. Manescau, S. D'Odorico, M. T. Murphy, T. Kentischer, W. Schmidt, and T. Udem, "Laser frequency combs for astronomical observations," Science **321**, 1335–1337 (2008).
3. P. Del'Haye, A. Schliesser, O. Arcizet, T. Wilken, R. Holzwarth, and T. J. Kippenberg, "Optical frequency comb generation from a monolithic microresonator," Nature **450**, 1214–1217 (2007).
4. A. Pasquazi, L. Caspani, M. Peccianti, M. Clerici, M. Ferrera, L. Razzari, D. Duchesne, B. E. Little, S. T. Chu, D. J. Moss, and R. Morandotti, "Self-locked optical parametric oscillation in a CMOS compatible microring resonator: a route to robust optical frequency comb generation on a chip," Opt. Express **21**, 13333–13341 (2013).
5. H. J. Jung, C. Xiong, K. Y. Fong, X. F. Zhang, and H. X. Tang, "Optical frequency comb generation from aluminum nitride microring resonator," Opt. Lett. **38**, 2810–2813 (2013).
6. M. A. Foster, S. L. Jacob, O. Kuzucu, K. Saha, M. Lipson, and A. L. Gaeta, "Silicon-based monolithic optical frequency comb source," Opt. Express **19**, 14233–14239 (2011).
7. T. Hansson, D. Modotto, and S. Wabnitz, "Dynamics of the modulational instability in microresonator frequency combs," Phys. Rev. A **88**, 023819 (2013).
8. I. H. Agha, Y. Okawachi, and A. L. Gaeta, "Theoretical and experimental investigation of broadband cascaded four-wave mixing in high-Q microspheres," Opt. Express **17**, 16209–16215 (2009).
9. A. Antikainen and G. Agrawal, "Dual-pump frequency comb generation in normally dispersive optical fibers," J. Opt. Soc. Am. B. **32**, 1705–1711 (2015).
10. Y. K. Chembo and N. Yu, "Modal expansion approach to optical-frequency-comb generation with monolithic whispering-gallery-mode resonators," Phys. Rev. A **82**, 033801 (2010).
11. T. Hansson, D. Modotto, and S. Wabnitz, "On the numerical simulation of Kerr frequency combs using coupled mode equations," Opt. Commun. **312**, 134–136 (2014).
12. X. H. Hu, Y. S. Liu, X. Xu, Y. Feng, W. F. Zhang, W. Q. Wang, J. Z. Song, Y. S. Wang, and W. Zhao, "Spatiotemporal evolution of a cosine-modulated stationary field and Kerr frequency comb generation in a microresonator," Appl. Opt. **54**, 8751–8757 (2015).
13. Y. K. Chembo and C. R. Menyuk, "Spatiotemporal Lugiato-Lefever formalism for Kerr-comb generation in whispering-gallery-mode resonators," Phys. Rev. A **87**, 053852 (2013).
14. A. B. Matsko, A. A. Savchenkov, D. Strekalov, V. S. Ilchenko, and L. Maleki, "Optical hyperparametric oscillations in a whispering-gallery-mode resonator: threshold and phase diffusion," Phys. Rev. A **71**, 033804 (2005).
15. T. Hansson and S. Wabnitz, "Bichromatically pumped microresonator frequency combs," Phys. Rev. A **90**, 013811 (2014).
16. D. V. Strekalov and N. Yu, "Generation of optical combs in a whispering gallery mode resonator from a bichromatic pump," Phys. Rev. A **79**, 041805 (2009).
17. E. Myslivets, B. P.-P. Kuo, N. Alic, and S. Radic, "Generation of wideband frequency combs by continuous-wave seeding of multistage mixers with synthesized dispersion," Opt. Express **20**, 3331–3344 (2012).
18. V. Ataie, E. Myslivets, B. P.-P. Kuo, N. Alic, and S. Radic, "Spectrally equalized frequency comb generation in multistage parametric mixer with nonlinear pulse shaping," J. Lightwave Technol. **32**, 840–846 (2014).
19. W. Q. Wang, S. T. Chu, B. E. Little, A. Pasquazi, Y. S. Wang, L. R. Wang, W. F. Zhang, L. Wang, X. H. Hu, G. X. Wang, H. Hu, Y. L. Su, F. T. Li, Y. S. Liu, and W. Zhao, "Dual-pump Kerr micro-cavity optical frequency comb with varying FSR spacing," Sci. Rep. **6**, 28501 (2016).
20. Y. Okawachi, M. J. Yu, K. Luke, D. O. Carvalho, S. Ramelow, A. Farsi, M. Lipson, and A. L. Gaeta, "Dual-pumped degenerate Kerr oscillator in a silicon nitride microresonator," Opt. Lett. **40**, 5267–5270 (2015).
21. M. Peccianti, A. Pasquazi, Y. Park, B. E. Little, S. T. Chu, D. J. Moss, and R. Morandotti, "Demonstration of a stable ultrafast laser based on a nonlinear microcavity," Nat. Commun. **3**, 765 (2012).
22. M. Ferrera, L. Razzari, D. Duchesne, R. Morandotti, Z. Yang, M. Liscidini, J. E. Sipe, S. Chu, B. E. Little, and D. J. Moss, "Low-power continuous-wave nonlinear optics in doped silica glass integrated waveguide structures," Nat. Photonics **2**, 737–740 (2008).
23. D. Duchesne, M. Ferrera, L. Razzari, R. Morandotti, B. E. Little, S. T. Chu, and D. J. Moss, "Efficient self-phase modulation in low loss, high index doped silica glass integrated waveguides," Opt. Express **17**, 1865–1870 (2009).
24. A. Haboucha, H. Leblond, M. Salhi, A. Komarov, and F. Sanchez, "Analysis of soliton pattern formation in passively mode-locked fiber lasers," Phys. Rev. A **78**, 043806 (2008).
25. X. Xue, Y. Xuan, P.-H. Wang, Y. Liu, D. E. Leaird, M. H. Qi, and A. M. Weiner, "Normal-dispersion microcombs enabled by controllable mode interactions," Laser Photon. Rev. **9**, L23–L28 (2015).